*Int. J. Heat Mass Transfer.* Vol. 36, No. 13, pp. 3251–3263, 1993
Printed in Great Britain

0017–9310/93 $6.00 + 0.00


# Onset of natural convection in a cube

W. J. HILLER, ST. KOCH and T. A. KOWALEWSKI
Max-Planck-Institut für Strömungsforschung, Bunsenstr. 10, W-3400 Göttingen, Germany

and

F. STELLA
Università di Roma *La Sapienza*, Via Eudossiana, 18-00184, Roma, Italy

(*Received* 30 *September* 1992 *and in final form* 21 *January* 1993)

**Abstract**—The problem of transient natural convection in a cube-shaped cavity is investigated experimentally and numerically. The motion is driven by a sudden temperature difference applied to two opposite side walls of the vessel. The experiments are performed at a Rayleigh number of $1.66 \times 10^5$ and a Prandtl number of 1109, inside a $5 \times 5 \times 5$ cm$^3$ cavity made of Plexiglas, with two isothermal copper walls kept at a prescribed temperature. Numerical simulation has been performed using a finite difference vorticity–velocity model of the Navier–Stokes equation with the Boussinesq approximation. The theoretical predictions are found to be in good agreement with the experimental results.

## 1. INTRODUCTION

THE TRANSPORT of heat or mass by a buoyancy-induced convective motion is a mechanism which is relevant to many physical systems; consequently numerous theoretical, experimental and numerical studies of various aspects of natural convection flows have been performed. In particular, the idealised case of steady laminar flow in an enclosed rectangular cavity with differentially heated end walls has been extensively studied in various contexts [1–4]. On the other hand, the unsteady behaviour is not so extensively documented even though the transitional flow is of importance in many real problems [5–7]. Perhaps this is due to the rather tedious numerical calculations and experimental difficulties arising in monitoring transient values of temperature and velocity fields in the whole cavity. The new experimental technique [8] making use of liquid crystal tracers as indicators of temperature and velocity, helps to master some of these problems.

The subject of the present paper is the experimental investigation of the response of an initially isothermal fluid in a cube-shaped container to an instantaneous change of the temperature of one of the vertical walls. The problem is encountered in many practical situations where heating or cooling devices are suddenly switched on, and also in many environmental applications, with characteristic time-dependent heating and cooling cycles. For comparison, a symmetrical heating process was also investigated in which the temperature of both side walls was suddenly changed.

Depending on the value of the Rayleigh number, at least three flow regimes of steady convection in the cavity can be established. At relatively small Rayleigh numbers ($Ra < 10^3$), heat transfer is mainly due to heat conduction in the medium, and the corresponding isotherms are nearly parallel to the heated walls. The horizontal temperature gradient is positive everywhere in this case, giving rise to a positive vorticity generation. The streamlines are those of a single spiral, with its centre being at the centre of the cavity. As the Rayleigh number increases ($Ra > 10^3$), the heat transfer due to convection begins to play a significant role, generating a vertical temperature gradient in the centre of the cavity. The horizontal gradient of temperature diminishes in the centre, and for a further increase in the Rayleigh number ($Ra > 6 \times 10^4$), becomes locally negative, leading to a reduction of vorticity in the core. This causes an elongation of the central streamlines in the horizontal direction and the development of a second spiral in the core. When the temperature difference between the isothermal walls (and with it the Rayleigh number also) was gradually increased, it was observed [9] that the flow changes its character from a single to a double spiral configuration, evidently without any critical regions separating the two flow structures. It seems that during the heating process, the system passes through all these phases of convection, before the final stable state is reached. The details of the way in which the flow structures are continuously modified and change their topological character still remain unclear. Therefore, it appears quite useful to perform supplementary experiments to investigate these details and understand better the transient behaviour of convective flows.

In the previous experimental study [9, 10] it was observed that the flow structures in the cube cavity are rather complicated, even in the steady case. In particular, the flow away from the vertical mid-plane of the cavity is strongly three-dimensional and differs strikingly from existing two- and three-dimensional

## NOMENCLATURE

| | | | |
|---|---|---|---|
| $B$ | blue colour signal | $\Delta T$ | temperature difference, $(T_h - T_c)$ |
| $\mathbf{g}$ | acceleration due to gravity [m s$^{-2}$] | $\mathbf{u}$ | dimensionless velocity vector |
| $G$ | green colour signal | $V$ | fluid velocity in $y$ direction [mm s$^{-1}$] |
| $I$ | intensity (luminance) | $x$ | dimensionless distance on $x$ axis |
| $l$ | cavity dimension [m] | $y$ | dimensionless distance on $y$ axis. |
| $Nu$ | Nusselt number | | |
| $Pr$ | Prandtl number | | |
| $R$ | red colour signal | Greek symbols | |
| $S$ | colour saturation | $\beta$ | thermal expansion of fluid [°C$^{-1}$] |
| $t$ | time [s] | $\kappa$ | thermal diffusivity [m$^2$ s$^{-1}$] |
| $T_c$ | temperature of the 'cold' wall [°C] | $\nu$ | kinematic viscosity [m$^2$ s$^{-1}$] |
| $T_h$ | temperature of the 'hot' wall [°C] | $\theta$ | dimensionless temperature |
| $T_0$ | initial temperature [°C] | $\omega$ | vorticity vector. |

numerical results. These differences are due mainly to the failure to achieve strictly adiabatic condition on the insulating side walls. Unfortunately, it seems impossible to find transparent and ideally adiabatic walls. Hence, in the present study we limit our interest to the mid-plane of the cavity, avoiding additional complications due to unknown thermal boundary conditions on the side walls.

Two computer-aided experimental techniques were used for simultaneous measurement of the temperature and velocity fields: analysis of the light colour (hue) which is reflected by the liquid-crystal tracers suspended in the flow, and Particle Imaging Velocimetry (PIV), respectively.

## 2. DESCRIPTION OF THE PROBLEM

We consider the convective flow in a cubic box filled with a viscous heat-conducting liquid. The fluid density is assumed to be only temperature dependent. Both the fluid and the cavity walls are initially in thermal equilibrium, having a temperature $T_0$. Two opposite, vertical walls of the cavity are isothermal, whereas the other four walls are thermal insulated (adiabatic). In the case of asymmetrical heating the temperature of the cold wall is kept at the initial temperature ($T_c = T_0$) and the temperature of the hot wall $T_h$ is suddenly increased at time $t = 0$ to $T_h > T_0$. Symmetrical heating is performed by simultaneously changing the temperatures $T_c$ and $T_h$ of the cold and hot walls in such a way that $(T_h + T_c)/2 = T_0$, the initial fluid temperature. Thereafter (i.e. at $T > 0$), the 'hot' isothermal wall maintains its temperature $T_h$ and the 'cold' wall, temperature $T_c$.

Due to the temperature gradient applied between the walls, the fluid inside the cavity initially at rest begins to move. At first, heat is conducted into the fluid from the hot wall, resulting in a vertical layer of heated fluid. The buoyancy forces act to accelerate the fluid, thus creating a vertical viscous layer with large velocities transporting liquid into the top of the cavity. Vorticity generated in this layer is transported away by this velocity and diffused into the core, later creating a secondary viscous layer. A double layer structure appears, with the inner thermal layer governed by a buoyancy–viscous balance, and the outer viscous layer by an inertia–viscous balance.

The scale analysis of Patterson and Imberger [5] shows that a number of types of the initial flow are possible, leading ultimately to one of two types of steady flow, namely, conduction dominant flow and convective flow. Which type occurs is determined by the relative values of the dimensionless parameters: Rayleigh number, Prandtl number, and, for a non-cubic cavity, the aspect ratio of the cavity.

At small Rayleigh number the flow is dominated by conduction, which is seen in the form of vertical isotherms travelling across the cavity. Convection is here negligible in comparison with the horizontal conduction of the heat. In the flow analysed here at $Ra = 1.66 \times 10^5$, both convection and conduction are significant. The steady state is achieved by combined effects of the thermal layers propagating from the isothermal walls, and convective effects generating horizontal isotherms in the core. The liquid transported along isothermal walls is forced by the horizontal boundaries of the cavity to change its direction and to flow into the core of the cavity. Since the core is initially isothermal (at the temperature $T_0$), the unheated fluid from the viscous layer discharges as a potential flow into the central part of the cavity, whereas the heated fluid from the thermal boundary layer moves along the top of the cavity. The motion in the core region is driven by the boundary layer flow and flow velocities there are very small compared with those in the upper layer. The loss of heat from the intruding upper-layer flow to the core is only by conduction, and is therefore small in comparison with the heat flux across the cavity.

The subsequent motion in the core region is

extremely complex. As time passes, the flow in the vertical boundary layers introduces heated fluid to distinct horizontal layers, which convect heat across the cavity without any significant loss by conduction. As subsequent layers traverse the core, a stable vertical temperature gradient is set up. The core fills up with the horizontally-layered heated fluid.

At high Rayleigh number, flow oscillations may also appear. The spreading horizontal upper flow layers interact with the vertical ones on the cold side of the cavity, inducing a tilting of the isotherms beyond the horizontal (two vortex convection regime). As pointed out by Patterson and Imberger [5], if the Rayleigh number is high enough ($Ra > Pr^2$), this 'overshooting' of the isotherms may induce generation of internal waves in the velocity and temperature fields before their steady state is reached.

## 3. NUMERICAL MODEL

The origin of a rectangular Cartesian coordinate system is located at the lower corner of the cavity; the hot and cold walls then have coordinates $x = 0$ and $x = 1$, respectively (dimensions are normalized by the cavity size). The numerical simulations of the problem have been performed using a finite differences model of the Navier–Stokes equations. The Boussinesq approximation has been used in the numerical model and the equations are written in the vorticity–velocity form [11]:

$$\frac{1}{Pr}\frac{\partial \boldsymbol{\omega}}{\partial t} + \frac{1}{Pr}\nabla \times (\boldsymbol{\omega} - \mathbf{u}) = \nabla^2 \boldsymbol{\omega} - Ra \nabla \times \left(\theta \frac{\mathbf{g}}{|\mathbf{g}|}\right) \quad (1)$$

$$\nabla \cdot \mathbf{u} = 0 \quad (2)$$

$$\frac{\partial \theta}{\partial t} + (\mathbf{u} \cdot \nabla)\theta = \nabla^2 \theta. \quad (3)$$

The standard conservative form is adopted for the convection terms in the vorticity transport equation in order to conserve exactly the mean vorticity as prescribed by the Stokes theorem. Furthermore this form for the convective terms reduces numerical instabilities.

The dimensionless parameters $Ra$ and $Pr$ defining the problem then follow:

$$Ra = \frac{\mathbf{g}\beta \Delta T l^3}{\kappa \nu}$$

$$Pr = \frac{\nu}{\kappa};$$

and the vorticity is defined as

$$\boldsymbol{\omega} = \nabla \times \mathbf{u}. \quad (4)$$

In the above definitions, $\mathbf{g}$, $l$, $\Delta T$, $\kappa$, $\beta$, $\nu$ denote gravitational acceleration, cavity dimension, wall temperatures difference, thermal diffusivity, coefficient of thermal expansion and kinematic viscosity, respectively.

The equations for the velocities are obtained by taking the appropriate derivatives of vorticity (4) and using the continuity equation (2). This yields the Poisson type equation:

$$\nabla^2 \mathbf{u} = -\nabla \times \boldsymbol{\omega}. \quad (5)$$

The complete set of equations used in the numerical simulation consists of equations (1), (5) and (3).

### 3.1. *Boundary conditions*

The formulation used in terms of vorticity–velocity variables leads to a very simple way of enforcing the boundary conditions for the chosen variables. The boundary condition associated with equation (1) is the vorticity definition (4) written on the boundary. The boundary conditions associated with the elliptic velocity equation (5) are the velocity components equal to zero on the solid walls. The boundary conditions imposed on the energy equation are:

$$\theta = 1 \quad \text{at} \quad x = 0,$$

$$\theta = 0 \quad \text{at} \quad x = 1,$$

$$\frac{\partial \theta}{\partial n} = 0 \quad \text{at} \quad y = 0,$$

$$\frac{\partial \theta}{\partial n} = 0 \quad \text{at} \quad y = 1.$$

To speed-up the numerical calculation, the three dimensional code was run only for the centre plane of the cavity. A uniform staggered mesh of the size $61 \times 61 \times 3$ has been applied in the calculations, where the last dimension is used solely to satisfy the boundary conditions for the third coordinate ($z$), i.e. slip of the velocity and zero heat and the flow flux through the boundary. The mesh size was chosen after the performance of several tests in which its size was increased from $21 \times 21 \times 3$ to $61 \times 61 \times 3$. It was found that for the flow conditions investigated there is no significant change in the flow generated once the main mesh dimension is increased beyond 41.

In the additional test 3-D calculations with a mesh size $61 \times 61 \times 61$ have been performed for the final state, imposing adiabatic thermal boundary conditions on all but isothermal walls. The results have been compared with similar calculations using the false-transient code FRE-CON3D [12]. It was found that both 3-D results are the same (with accuracy presumed in the calculations). Also, there are no meaningful differences between the temperature and velocity fields generated for the centre plane of the cavity when using 2-D and 3-D calculations. Therefore, the assumption that 2-D calculations are sufficient to describe the flow in the centre plane of the cavity seems to be fully justified.

### 3.2. *Unsteady algorithm*

A time-dependent algorithm has to be used to solve the transient heating of the cavity. The real transient procedure requires particular attention when used

together with the vorticity–velocity formulation. In fact because the continuity equation is imposed only in an implicit way, mass conservation and consistency of vorticity definition could be violated if a good coupling between the full set of the equations used is not ensured. In the present work the required coupling has been achieved by an inner iteration of all the governing equations for each time step, as proposed also in ref. [13].

## 4. EXPERIMENTAL APPARATUS

The experimental set-up used for measuring temperature and velocity fields is shown schematically in Fig. 1. It is essentially similar to that one previously used [9, 10]. The convection cavity, the xenon flash tube and the camera are mounted on a rectangular frame, which can be tilted to observe vertical and horizontal cross-sections without re-adjusting the optics. The box, of inner length 50 mm, consists of two vertical isothermal walls, opposite each other, made of black anodized metal, and four 8 mm thick Plexiglas walls. Each of the isothermal walls is maintained at constant temperature by a water flow which passes through internal passages in the plates. The temperature of the water is controlled by a thermostat. The heating (or cooling) of the side walls is started abruptly by opening the inlet valves to the water passages. The temperature of both isothermal walls was $T_c = 20$°C and $T_h = 23$°C, respectively. The initial temperature of the fluid $T_0$ was 20°C (or 21.5°C for the symmetrical case). The outside air temperature was $22 \pm 1$ C. These temperatures were monitored continuously by means of thermocouples and recorded by a Philips multichannel recorder (PM8238). The end walls reached their operating temperatures within about 15 s. Thereafter, temperature control within 0.1 C was possible.

The Rayleigh number based on the cavity size was $1.66 \times 10^5$. An aqueous solution of glycerin (approximately 87% glycerin) was employed as a flow medium; the Prandtl number was 1109. The temperature and velocity fields were measured by means of liquid crystals (LC) suspended as small tracer particles in the liquid. The LC which we used here are chiral nematics type TM317 (BDH Chemicals Ltd.).

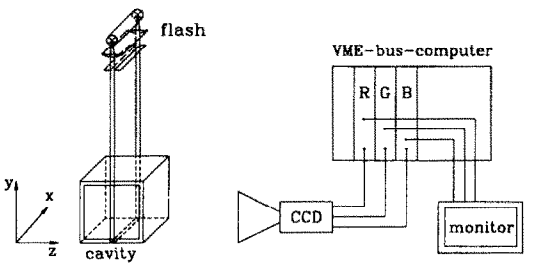


FIG. 1. Scheme of the experimental set-up. The CCD colour camera observes the centre plane of the cavity, illuminated by the vertical light sheet.

The visualisation of temperature using thermochromic liquid crystals is based on their temperature-dependent refractivity at the wavelengths of visible light. If the liquid crystals are illuminated with white light, then the colour of the light they reflect changes from red to blue when the temperature is raised. This happens in a well defined temperature range (the so called colour play range), which depends on the type of LC used.

The flow is observed at the centre vertical $X$–$Y$ cross sections of the cavity using a light sheet technique. The xenon flash tube generates a 2 mm thick sheet of white light, which illuminates the cross-section of the flow. The wavelength (colour) of the observed reflected light depends on the temperature of the LC-tracers and also on the angle of observation. Therefore, special care must be taken to minimize errors produced by wide angle lenses and inaccurate matching of the angle between the camera and the light source.

The three chip CCD colour camera (Sony DXC-750P), which gives an RGB-signal for the red, green and blue portions of the incoming light, is used to observe the flow. The images are acquired by three identical 8-bit frame grabbers (PPI-Eltec) in a VME-bus computer.

The recording of the flow patterns and temperature fields is performed periodically (every 30–60 s), beginning 1 min after the start of heating. The recorded digitized images are stored on the hard disk of the computer for later evaluation.

Besides the further image processing, the computer also controls the experimental conditions, i.e. the wall temperatures, position of the cavity and recording sequences. By moving the convection cavity perpendicular to the light sheet it is possible to scan the temperature and velocity fields of the entire flow.

### 4.1. *Temperature measurements*

As previously mentioned, the cavity is filled with a very dilute suspension of uncoated thermochromic liquid crystal droplets in a glycerin–water mixture. The mean diameter of LC-droplets is about 50 $\mu$m. LC-particles are used both as tracers for the velocity evaluation and as local temperature sensors. For evaluating the temperature the generally applied [14, 15] *HSI* representation of the *RGB* space is used. The incoming *RGB* signals are transformed pixel by pixel into intensity, saturation and hue. Temperature is determined by relating the hue to a temperature calibration function.

The values of intensity, saturation and hue are computed with a quite simple and fast algorithm, which nevertheless gives the same accuracy as other more complex formulae. For the given three values of $R$, $G$ and $B$, the intensity is defined as

$$I = \sqrt{(R^2 + G^2 + B^2)}$$

and the saturation as

$$S = 1 - \min(R, G, B)/I.$$

The hue is the ratio of those two values of $(R, G, B)$, which, after subtracting min $(R, G, B)$ are non-zero.

In practice, by 8-bit discretisation of the *RGB* signals from the TV-camera, the value of hue varies on the chromaticity diagram over the range 0–252. The pure *RGB* colours are then at 0 (and 252) for red, 84 for green and 168 for blue, with all mixed colours (i.e. red–green, green–blue and blue–red) having intermediate values. As liquid crystals reflect pure spectral colours, there are no hue values registered simultaneously by the blue- and red-sensitive chips of the camera. Hence, only the *R–G* and *G–B* hue regions of the chromaticity diagram have to be considered. Consequently, it is convenient to expand the whole *R–B* hue range to cover the values 0–252, thus improving the colour (i.e. temperature) resolution of the method.

The calibration is performed at the experimental conditions, by gradually increasing the temperature in the entire uniformly heated cavity (in steps of 0.1 K), and evaluating the hue of light reflected from tracers close to the isothermal walls. The non-linear relation between temperature and hue (predetermined by the camera construction) is described by a 9th order polynomial fitted to the points (Fig. 2) measured for LC type TM317 (BDH). The accuracy of the measured temperature depends on the hue value, and varies in the temperature range 20–24°C from $\pm 0.1$ to $\pm 0.3$ K.

The limited spatial resolution of the camera, errors due to amplitude discretisation of the video signals, non-uniformity of the illumination and also the presence of 'degenerated' liquid crystals (giving false colour response due to their chemical degradation) are only a few of the possible reasons that the accuracy of the method for the point measurements is relatively low. Therefore, to minimize these effects recorded information must first be processed by interpolating and averaging signals of the single pixels. Consequently, the averaging of the images has been performed with a median filter over an area of $5 \times 5$ pixels, whereas 'black' regions without colour information have been 'filled up' by interpolation. After evaluation of the colour of such pre-processed images, results can be displayed as a false-colour image for direct estimation of the temperature distribution, and reproduced in the form of a temperature map (isotherms) by means of a plotting program.

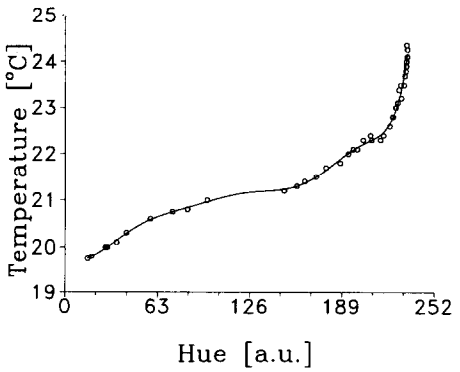


FIG. 2. Calibration curve of temperature as a function of the hue values evaluated from the light reflected by the liquid crystals suspended in the working fluid. Observation at right angles to the direction of the incident light.

### 4.2. *Velocity measurements*

The 2-D velocity vector distribution has been measured by particle image velocimetry (PIV). By this method the motion of the scattering particles observed in the plane of the illuminating light sheet can be analysed. Usually PIV techniques apply an autocorrelation method for doubly-exposed photographic images. It offers high temporal resolution, but the analysis gives only the length and angle of the displacement vector, and not its sign. The method applied here [16], uses two separately captured digital images taken at a constant time interval (typically 5 s) to evaluate the motion of the particles. Each of the images taken shows a relatively dense cloud of single illuminated particles (LC). The magnitude and direction of the velocity vectors is determined using a correlation analysis. This is done by dividing the whole image (typically $512 \times 512$ pixels) into $64 \times 64$ pixel matrices, which are spaced every 32 pixels (partly overlapping each other). The correlation of corresponding matrices of both images allows the evaluation of the mean translation vector for each group of particles simultaneously detected in both matrices. The evaluation of images has been performed on an 80386 (25 MHz) personal computer equipped with the 32-bit signal processor DSP23CP (AT&T). The analysis of one pair of images takes about 20 min.

Compared with point measurement methods (such as Laser Doppler Velocimetry) the PIV technique used is less accurate and has a relatively low spatial resolution. This is mostly due to the low resolution of the CCD cameras. Hence, the results achieved give only a rough description of the local values of the velocity. However, the method has a supreme advantage for transient flows, offering simultaneous measurement of the velocity field in the entire cross-section illuminated by the light sheet. As the images of LC-tracers are also used to determine their colour (temperature), the experiment can be easily run even more simply using only a colour TV-camera, a good quality video-recorder, and a flash-light. This fact allows a direct application of the method in many practical engineering or environmental heat-transport measurements. The whole analysis can be performed afterwards, using the recorded video-tape material (although in this case some further loss of resolution must be taken into account).

## 5. RESULTS

Observation of the flow is limited to the centre-vertical plane of the cavity (i.e. $z = 0.5$), since a simultaneous observation of different cross-sections of the cavity is not possible at the present time. The experiment starts when a sudden temperature jump is applied to one (or both) isothermal, vertical walls of the cavity.

A few isotherms captured at four different instants, normalized by the applied temperature difference (20–23°C), are displayed in Fig. 3. The corresponding calculated isotherms are shown in Fig. 4. The isotherms correspond to the boundaries between ten isothermal regions defined within the temperature range being considered. Figures 5 and 6 show for the same instants the measured and calculated velocity fields.

The above illustrated asymmetrical case corresponds to the temperature jump applied to the hot wall. The isotherms show how the flux of heat from the hot wall into the adjacent fluid layer gradually generates convective flow in the whole cavity. The initially dominant conductive heating, characterised by almost vertical isotherms, is gradually replaced by convection. The velocity field is strongly asymmetrical, with a strong vertical component close to the hot wall (Figs. 5 and 6). The viscous layer which is generated, is relatively small and there is practically no flow in the core. After about 5 min (Figs. 3(b) and 5(b)) the effect of convection becomes evident. Particles near the side walls closely follow the form of the cavity. In the centre one vortex appears, surrounded by concentric streamlines along which fluid is transported from the core to the adjacent walls (compare with Fig. 11(a)).

The isotherms are gradually deformed by convection and begin to approach the characteristic S-shape. In the vicinity of the side walls, the temperature gradients are largest and the isotherms are nearly vertical. Close to the top and bottom walls, their pattern is further influenced by the thermal boundary conditions. In the interior region almost horizontal, regularly spaced isotherms appear. As time proceeds (after about 15 min) a well-developed typical convective structure of isotherms is seen. At this point a second much slower transition of the flow begins. We observe first a horizontal elongation of the streamlines and then the formation of a secondary vortex with its centre shifted towards the hot wall. The temperature field changes very little, although characteristic nega-

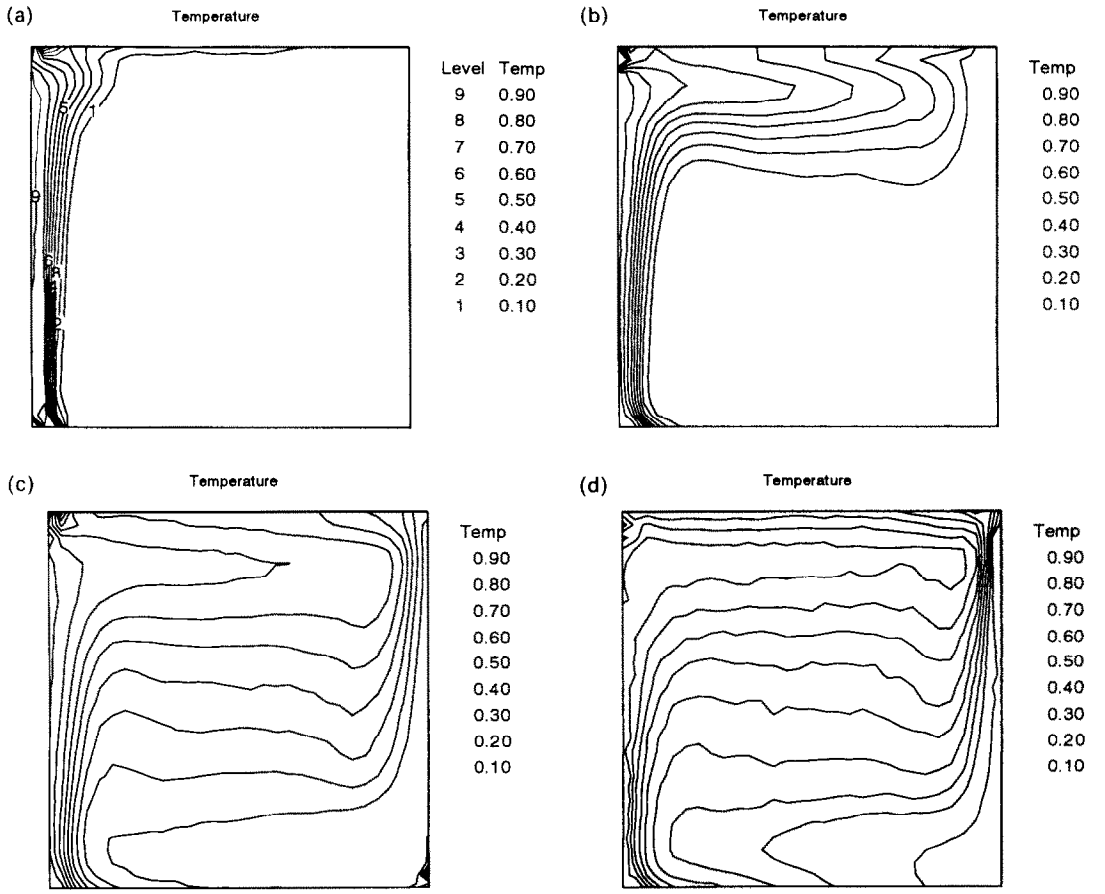


FIG. 3. Isotherms measured in the centre-plane of the cavity: (a) 1 min, (b) 5 min, (c) 20 min and (d) 2 h after the temperature jump is applied to the 'hot' wall.

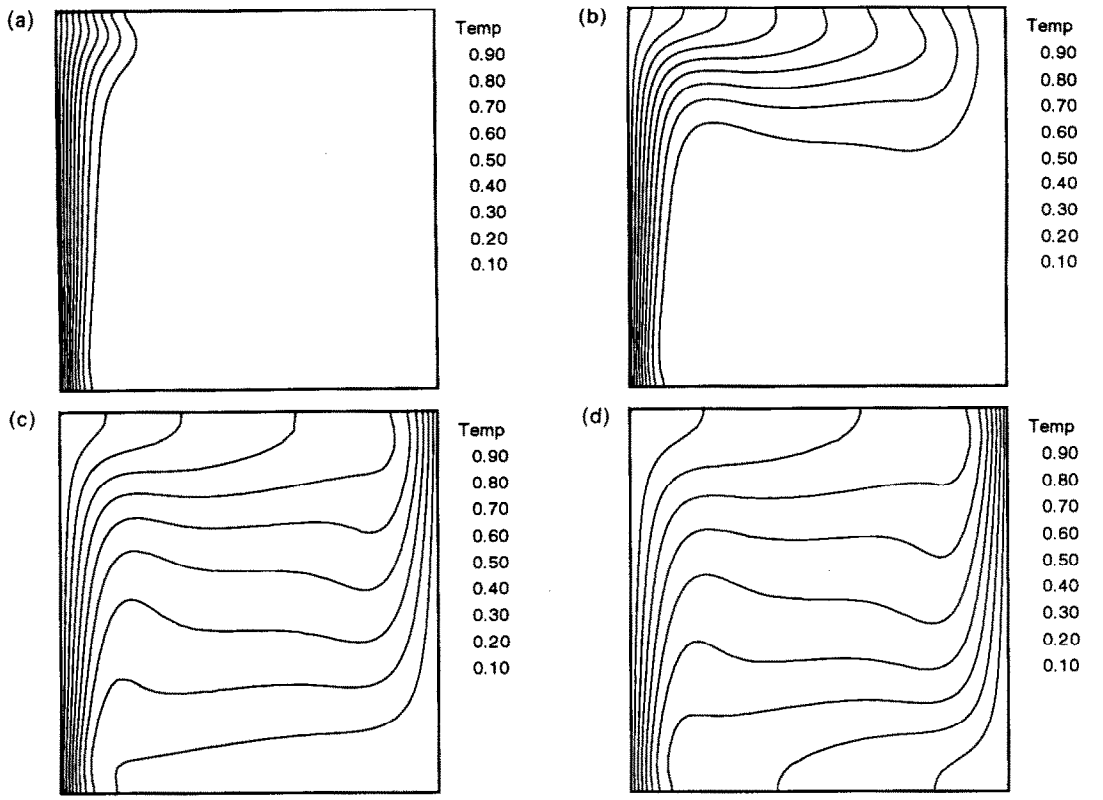


FIG. 4. Calculated isotherms for the case in Fig. 3: (a) 1 min, (b) 5 min, (c) 20 min and (d) final state.

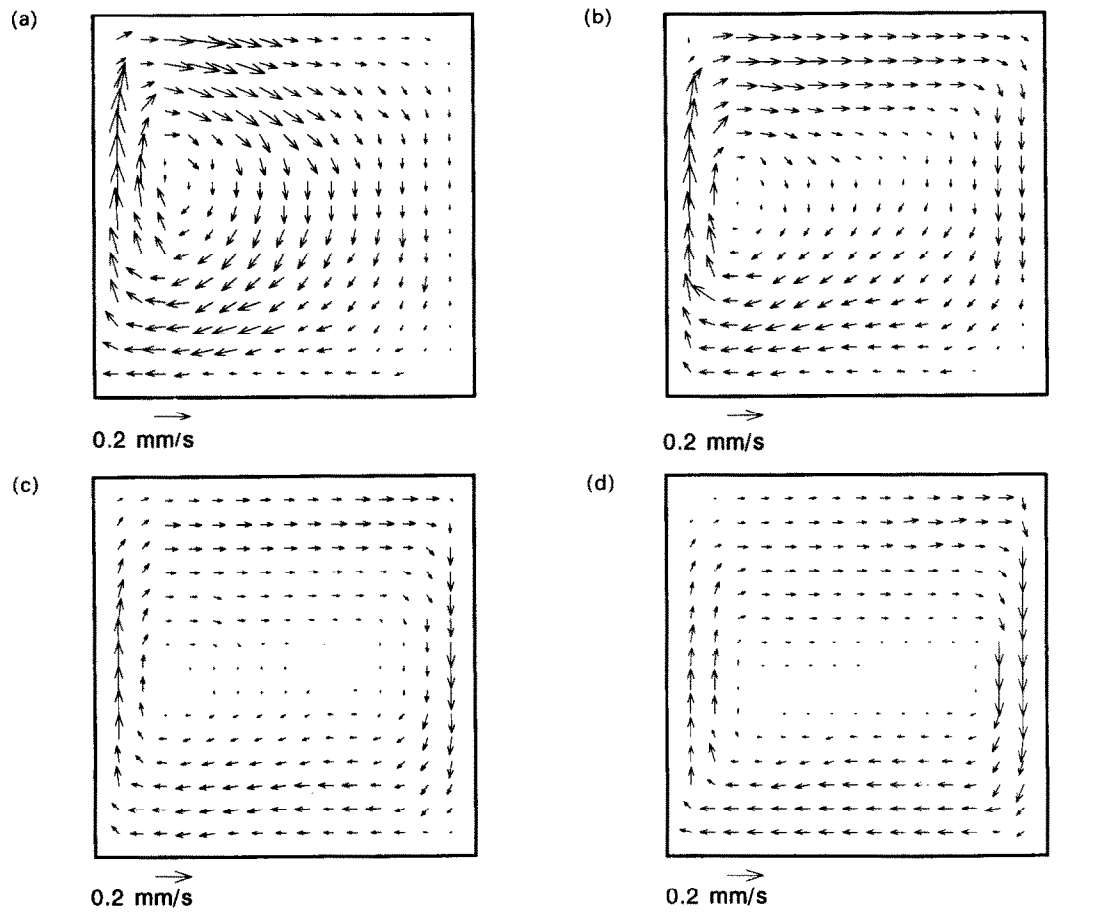


FIG. 5. Velocity field measured in the centre-plane of the cavity: (a) 1 min, (b) 5 min, (c) 20 min and (d) 2 h after the temperature jump is applied to the 'hot' wall.

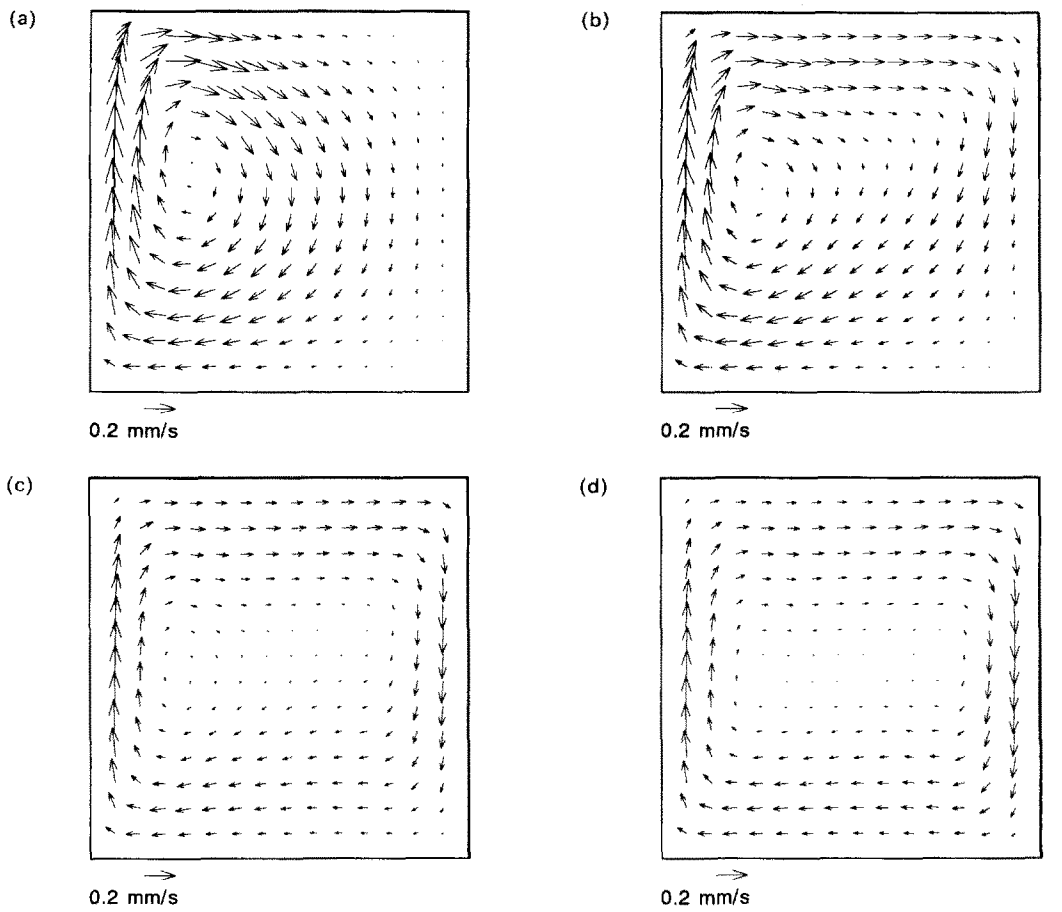


FIG. 6. Calculated velocity vectors for the case in Figs. 3–5: (a) 1 min, (b) 5 min, (c) 20 min and (d) final state.

tive tilting of the isotherms is now well developed. The two-vortex configuration can be clearly recognised after about 30 min, whereas asymptotic changes in the isotherms and flow pattern are still taking place. The final state is effectively reached after about 1 h. After this time the flow seems to be stable, and the velocity field becomes symmetrical (see also Fig. 11(c)).

Figure 7 shows experimental and calculated vertical velocity profiles at the centre line ($y = 0.5$). It can be seen, that during the first time period the vertical velocity close to the hot wall is almost 50% higher than its final value. The flow in the hot viscous layer accelerates very quickly after the temperature jump has been applied. In the case investigated the velocity field reaches its absolute maximum after about 2 min (compare Fig. 8). Later the viscous layer begins to spread out into the core region and the value of maximum velocity gradually drops. The temporal behaviour of the maximum flow velocity is displayed together with heat fluxes (given as Nusselt numbers for a few $Y$–$Z$ planes). It can be seen that the velocity maximum coincides with an overshoot of the Nusselt number. Apparently at the beginning of the heating process almost the entire heat flux from the hot wall is used to accelerate the liquid in the adjacent viscous layer. The asymptotic behaviour of the Nusselt numbers displayed in Fig. 8 provides evidence that after about 1 h the flow approaches its final state, evidently without any oscillations.

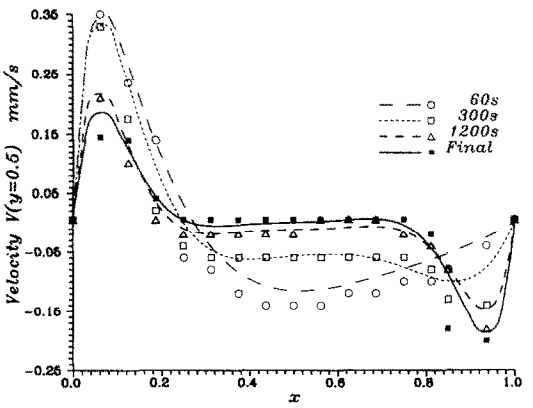


FIG. 7. Vertical velocity profiles at the centre line $y = 0.5$; times of 1 min, 5 min, 20 min after heating starts and the final state. Lines—calculation, points—experiment.

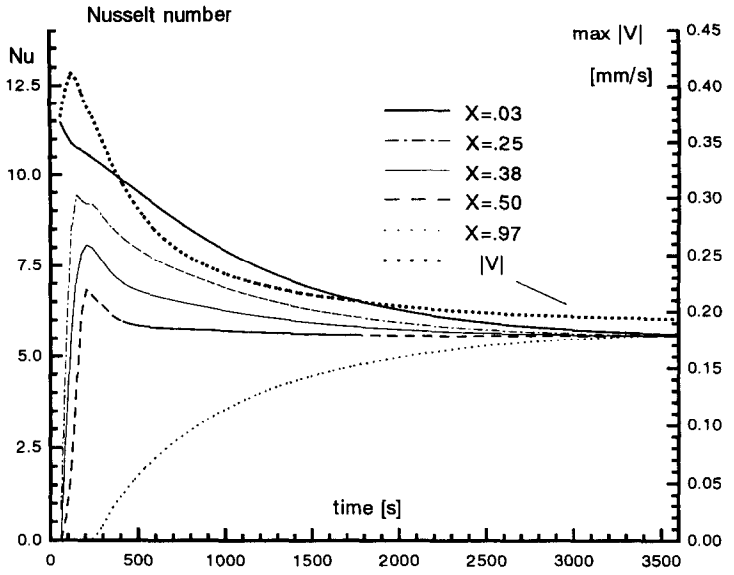


FIG. 8. Nusselt numbers calculated for the $X$-planes 0.03, 0.25, 0.38, 0.5, 0.97, and calculated absolute maximum of the vertical velocity $|V|$ as a function of time. Calculations performed for asymmetrical heating of the cavity.

The calculated and measured fields show generally good agreement. Some of the differences between measured and calculated temperature fields, which are most pronounced close to the top and bottom walls, are believed to be due to the final heat conduction within the walls. The wall conduction becomes especially important when the final state is approached. Small convective heat fluxes are then easily influenced by the thermal disturbances caused by non-adiabatic walls.

Furthermore, the LC-particles being less dense often collect at the top wall during the experimental run. The light from the flash scattered from the top wall covered with such a layer produces additional colour signals causing misleading local performance of the interpolation procedure. Also, the observed 'oscillations' of isothermal lines or the appearance of small iso-temperature 'islands' are due to inaccuracies in averaging signals from the single pixels by the interpolation algorithm rather than to a real physical phenomenon. This results mainly from the limited resolution of the method, which for the case analysed is equal to the distance between two adjacent isotherms (i.e. 0.3°C).

By comparing the velocity fields displayed in Figs. 5(b) and 6(b), it can be seen that the centre of the vortex created near the 'hot' wall is closer to the wall in the experiment than in the calculation. This may be due to the variable liquid viscosity, which is assumed to be constant in the numerical simulation. Over the temperature range applied in the experiments the viscosity of the liquid used varies by about 25% with temperature.

The local values of the vertical velocity extracted form the measured velocity fields are given for comparison with the calculated ones in Fig. 7. There is a good agreement of the initial values of the velocity, but the final state shows some discrepancies. In particular, the velocity measured close to the hot wall is lower than its cold counterpart. This effect, systematically observed, is probably also caused by non-ideal thermal boundary conditions on the top and bottom walls.

The symmetrical case, with simultaneously heating and cooling of opposite isothermal walls, is shown in Figs. 9 and 10. The final state, not shown in the figures, is the same as in the asymmetrical case. Compared with the previous case, both the isotherms and the velocity field show a smoother development. The flow develops symmetrically, quickly giving rise to the generation of a negative horizontal temperature gradient in the core. It causes the elongation of the central streamlines and the development of the double spiral system from the very beginning. The overshoot of the vertical velocity reaches only about 20% of its final value. The isotherms create their horizontal layers relatively quickly. This fast progressing of the flow perhaps explains why the isotherms measured after the first minute (Fig. 9(a)) are apparently 'ahead' of the calculated ones. The finite time, which the water from the thermostat needs to warm up the heating plates, has probably been over-predicted in that case.

The final state is effectively reached after about only 20 min. The differences between asymmetrical and symmetrical heating of the cavity can also be seen in Figs. 11(a)–(c), where the streamlines for the initial state are compared with their final shape.

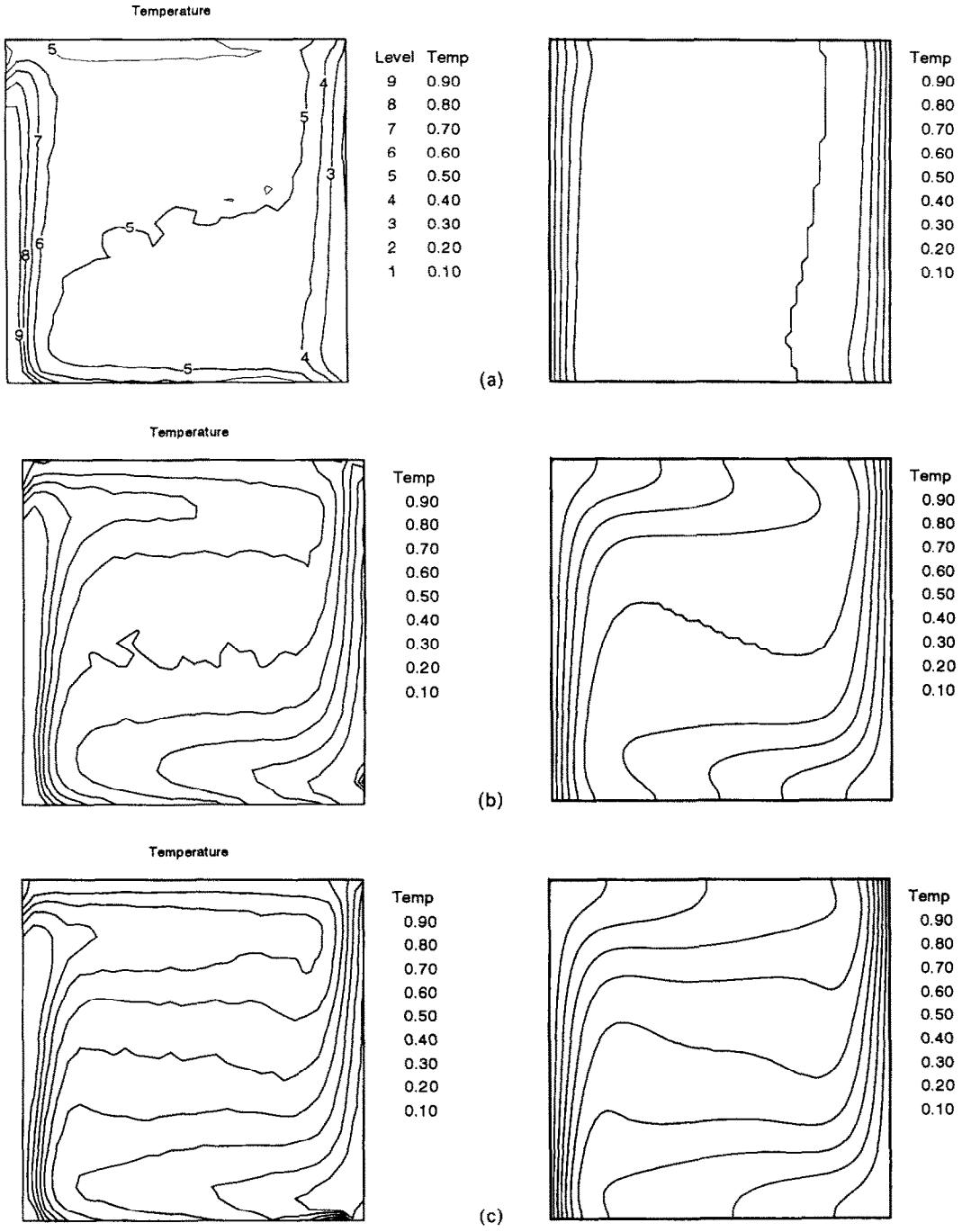


FIG. 9. Measured (left) and calculated (right) isotherms in the centre-plane of the cavity: (a) 1 min, (b) 5 min, (c) 10 min after the temperature jump is applied to the 'hot' and 'cold' walls (symmetrical heating).

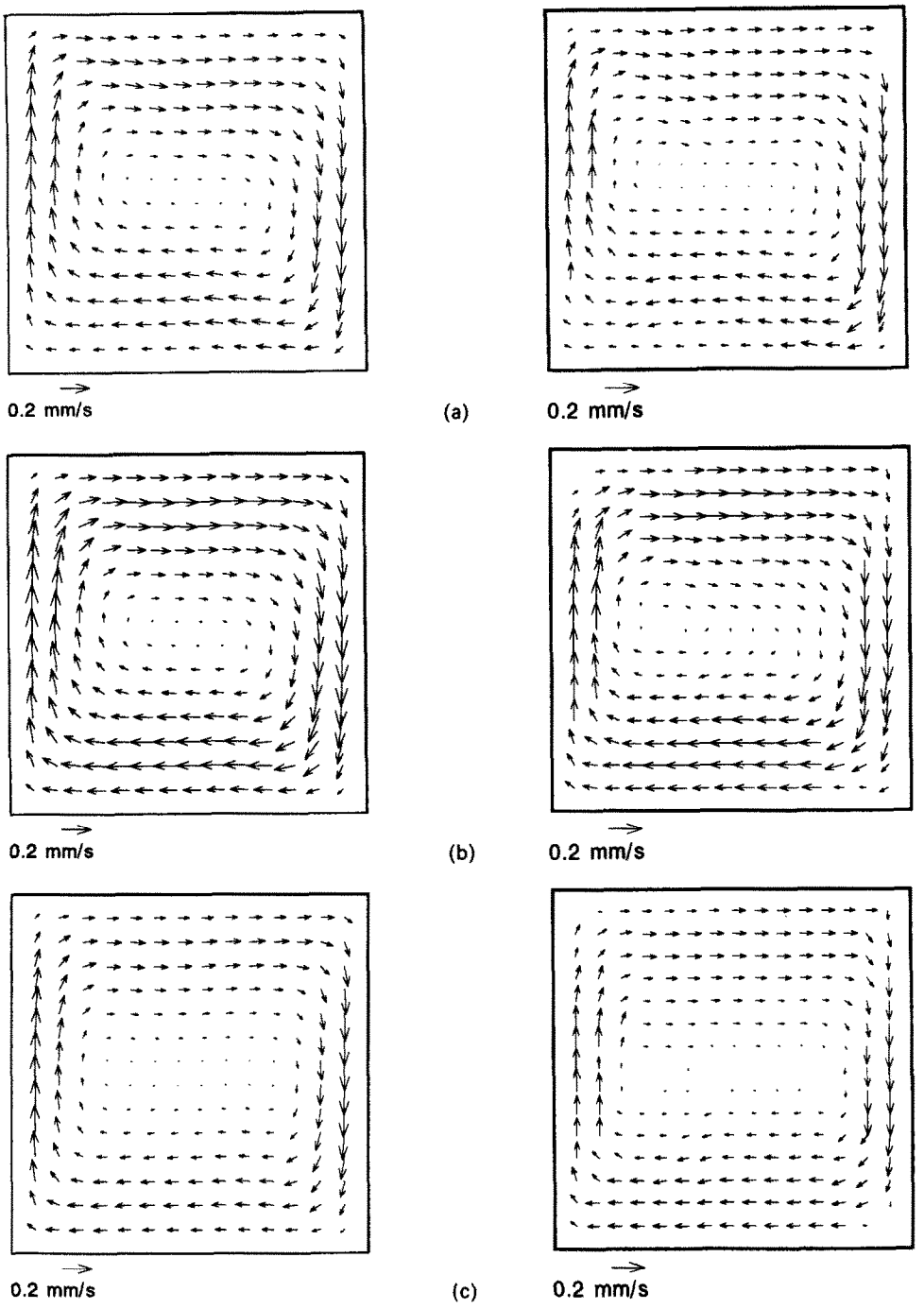


FIG. 10. Measured (left) and calculated (right) velocity fields for the case in Fig. 9: (a) 1 min, (b) 5 min, (c) 10 min.

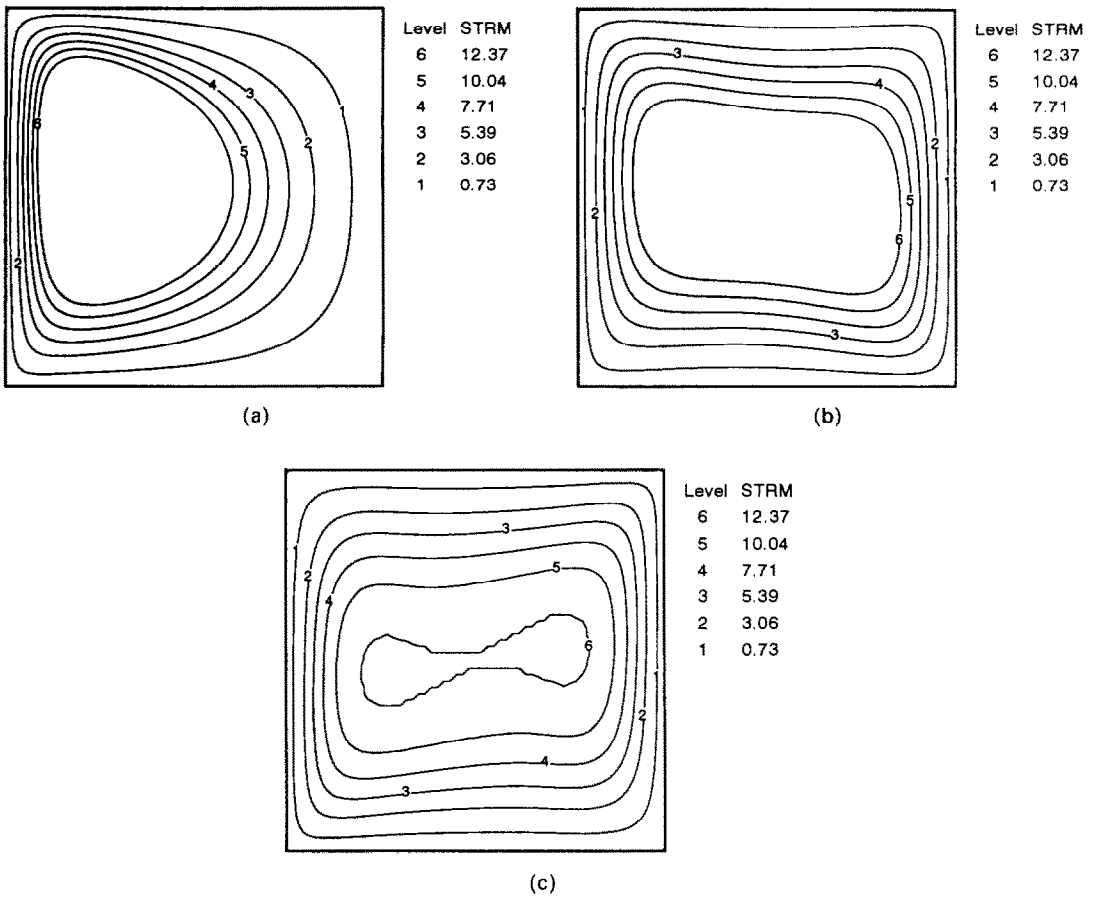


FIG. 11. Calculated streamlines: (a) asymmetrical heating—after 1 min, (b) symmetrical heating—after 1 min, (c) final state.

## 6. FINAL REMARKS

The system of simultaneous measurement of the flow and temperature fields based on the colour information from unencapsulated liquid crystal tracers has been successfully applied to visualise the onset of convection in a cube-shaped cavity. The experimental results are generally in good agreement with the numerical simulation, giving evidence of the validity of both approaches.

Both applied experimental methods are relatively imprecise as compared with the 'point' methods (such as those based on thermo-couples or LDA); nevertheless they offer the unique possibility of obtaining a general description of the transient flow and temperature fields. This allows direct comparison with numerical results and facilitates the identification of possible sources of discrepancy resulting from non-ideal experimental conditions (e.g. non-adiabatic side walls). A further improvement of the numerical modelling is then possible using a prescribed temperature distribution (instead of adiabatic conditions) for the non-isothermal walls. The colour analysis of non-isothermal walls coated with the liquid crystals offers the possibility of measuring the temperature on the inner side. In a separate study of the three-dimensional stationary case [17] it was found that imposing the measured temperature distribution on the walls as the boundary condition in the computational code [12] drastically reduces the severe discrepancies obtained for the calculated particle tracks. This gives good prospects for future modelling of the transient development of three-dimensional flow structures, which are very sensitive to thermal boundary conditions defined on the four non-isothermal walls of the cavity.

## REFERENCES

1. G. K. Batchelor, Heat transfer by free convection across a closed cavity between vertical boundaries at different temperatures, *Q. Appl. Math.* **12**, 209–233 (1954).
2. J. W. Elder, Laminar free convection in a vertical slot, *J. Fluid Mech.* **23**, 77–98 (1965).
3. G. de Vahl Davis, Laminar natural convection in an enclosed rectangular cavity, *Int. J. Heat Mass Transfer* **11**, 1675–1693 (1968).
4. G. D. Mallinson and G. de Vahl Davis, Three-dimensional natural convection in a box: a numerical study, *J. Fluid Mech.* **83**, 1–31 (1977).
5. J. Patterson and J. Imberger, Unsteady natural convection in a rectangular cavity, *J. Fluid Mech.* **100**, 65–86 (1980).

6. F. H. Bark, F. Alavyoon and A. A. Dahlkild, On the unsteady free convection in vertical slots due to prescribed fluxes of heat or mass at the vertical walls, *J. Fluid Mech.* **235,** 665–689 (1992).
7. C. G. Jeevaraj and J. C. Patterson, Experimental study of transient natural convection of glycerol–water mixtures in a side heated cavity, *Int. J. Heat Mass Transfer* **35,** 1573–1587 (1992).
8. W. Hiller and T. A. Kowalewski, Simultaneous measurement of the temperature and velocity fields in thermal convective flows. In *Flow Visualization IV* (Edited by Claude Veret), pp. 617–622. Hemisphere, Paris (1987).
9. W. J. Hiller, St. Koch and T. A. Kowalewski, Three-dimensional structures in laminar natural convection in a cube enclosure, *Exp. Therm. Fluid Sci.* **2,** 34–44 (1989).
10. W. J. Hiller, St. Koch, T. A. Kowalewski, G. de Vahl Davis and M. Behnia, Experimental and numerical investigation of natural convection in a cube with two heated side walls, *Proc. of the IUTAM Symposium Cambridge U.K.*, 13–18 August 1989 (Edited by H. K. Moffat and A. Tsinober), pp. 717–726. CUP (1990).
11. G. Guj and F. Stella, A vorticity–velocity method for the solutions of 3D incompressible flows, submitted to *J. Comp. Phys.* (1992).
12. L. P. Goh, E. Leonardi and G. de Vahl Davis, FRECON3D—Users Manual. A program for the numerical solution of mixed convection in a three-dimensional rectangular cavity, The University of New South Wales, School of Mech. and Ind. Eng., Rep. 1988/FMT/7, NSWU (1988).
13. H. Fasel, Investigation of the stability of boundary layer by a finite-difference model of the Navier–Stokes equations, *J. Fluid Mech.* **78,** 355–383 (1976).
14. C. Hirsch, K. H. Platzer, D. E. Metzger and S. Witting, Instationäre Wärmeübergangsmessung unter Nutzung von thermochromen Flüssigkristallen als Temperaturindikatoren. In 2D-Meßtechnik, DGLR-Workshop, 18–19 October 1988, Markdorf. Bericht 88-04, pp. 211–212. DGLR Bonn (1988).
15. K.-H. Platzer, C. Hirsch, D. E. Metzger and S. Wittig, Computer-based areal surface temperature and local heat transfer measurements with thermochromic liquid crystals (TLC), *Exp. Fluids* **13,** 26–32 (1992).
16. R. Paul, Die Erfassung von Geschwindigkeitsfeldern durch automatische Bewegungsanalyse am Beispiel einer rotierenden Flüssigkeit (Edited by E.-A. Müller), Mitteilungen aus dem MPI Göttingen FRG, No. 102 (1991).
17. W. J. Hiller, St. Koch, T. A. Kowalewski, K. Range, M. Behnia and G. de Vahl Davis, Visualization of 3-D natural convection—comparison with numerical results. In *Proc. of 11th ABCM Mech. Eng. Conf.*, São Paulo (Brasil), December 1991, Ed. Esp. de Revista Brasileira de Ciências Mecânicas, Vol. 2, pp. 21–24, São Paulo (1991).